LARGE DEFORMATIONS ON ELONGATED BODIES

De Nayer Guillaume, Visonneau Michel, Leroyer Alban
Ecole Centrale Nantes, Nantes, France

Boyer Frederic
Ecole des Mines de Nantes, Nantes, France

ABSTRACT

In this paper the coupling of a structural solver for elongated structures in large deformations and in large displacements with the flow solver ISIS-CFD is presented. ISIS-CFD is a 3D finite volume solver based on the incompressible unsteady Reynolds-averaged Navier-Stokes equations. The finite element structural solver is also 3D and uses Euler-Bernoulli or Rayleigh kinematics with the Cosserat hypothesis. A remeshing procedure based on the pseudo-solid approximation is detailed. This coupled algothim is first validated and then applied to a geometrically simple 2D test case.

1. INTRODUCTION

Elongated structures, like pillars supporting oil platforms or cables and risers, are frequently met in the industrial domain. The stakes of the fluid/structure interaction (FSI) around these bodies are therefore important. This is the reason why the CFD team of the Fluid Mechanics Laboratory from Centrale Nantes has started the development of FSI for elongated structures with the help of its in-house RANSE solver ISIS-CFD.

To carry out FSI modelling, four points are essential to address :

- The transfer of the efforts exerted by the fluid on the structure,
- The transfer of structure displacements to the fluid field,
- The fluid domain remeshing,
- The resolution of the dynamic structure problem.

2. ISIS-CFD, THE FLOW SOLVER

The ISIS-CFD flow solver, developed by the EMN (Equipe Modélisation Numérique) of the Fluid Mechanics Laboratory of the Ecole Centrale of Nantes, uses the incompressible unsteady Reynolds-averaged Navier-Stokes equations (RANSE). The solver is based on the finite volume method to build a spatial discretization of the transport equations. The face-based method is generalized to two-dimensional or three dimensional unstructured meshes for which non-overlapping control volumes are bounded by an arbitrary number of constitutive faces. The velocity field is obtained from the momentum conservation equations and the pressure field is extracted from the mass conservation constraint, or continuity equation, transformed into a pressure-equation. A second-order accurate three-level fully implicit time discretization is used. Surface and volume integrals are evaluated using second-order accurate approximation. In the case of turbulent flows, additional transport equations for modelled variables are solved in a form similar to the momentum equations and they can be discretized and solved using the same principles. Several turbulence models, ranging from the one-equation Spalart-Allmaras model (cf P. Spalart and S. Allmaras (1992)), two-equation $k-\omega$ closures (cf F.R. Menter (1993)), to a full stress transport $R_{ij}-\omega$ model (cf G.B. Deng and al (2005)), are implemented in the flow solver to take into account the turbulence phenomena.

3. FLOW FIELDS TRANFER BETWEEN SOLID AND FLUID MESHES

One of the difficulties in fluid/structure interaction is that the fluid and solid meshes do not match at the body boundary (cf A. de Boer et al. (2007)). In the special case of elongated structures, these ones are modelled by the beam theory. The solid grid is consequently the beam neutral line, whereas the structure is viewed from the fluid domain by a set of faces around this neutral line. In order to calculate the fluid efforts on

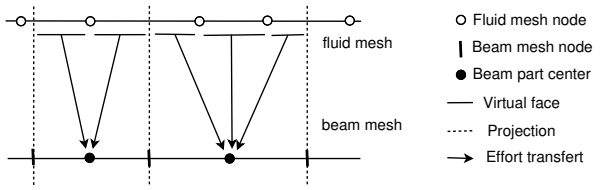

Figure 1: Fluid efforts interpolation on the beam

the beam, an interpolation is needed. The global conservation of the efforts being the most important property to fulfill, an ad-hoc interpolation has been developed.

The connectivities between fluid boundary-nodes and the beam sections are generated once at the launch of ISIS-CFD. They allow to determine to which part of the beam the orthogonal projection of the fluid boundary-nodes belongs. One has also the possibility to know the orthogonal projection of the beam nodes on the fluid boundary faces. With these data, the efforts are linearly interpolated. A fluid face, which entirely belongs to a beam section, provides the total fluid effort. In case of an orthogonal plane to a beam node cutting a fluid face, this one is virtually divided and the efforts are linearly distributed between the corresponding beam parts (cf fig. 1).

After the calculation of the beam deformation, this one is transmitted to the fluid grid with the same connectivities which were used before. The fluid mesh nodes which belong to the structure are displaced according to the beam kinematics.

4. FLUID DOMAIN REMESHING

At the end, the fluid mesh must be deformed in order to take into account the new beam position. ISIS-CFD integrates several remeshing tools. The first is an analytic regridding based on a weighting coefficient (cf fig. 2) which can be used with confidence for small and moderate deformations (cf A. Leroyer and M. Visonneau (2005)). Another regridding module has been developed in order to account for large deformations. This one is based on a pseudo-solid approach to build a consistent and robust unstructured grid deformation strategy. The fluid domain is considered as a linear elastic solid structure obeying structural equations which are linearised and used even in the case of large deformations since one does not need to follow the physics for this virtual elastic grid. The control parameters are the non-uniform Young modulus E, Poisson Coefficient μ and shearing coefficient G.

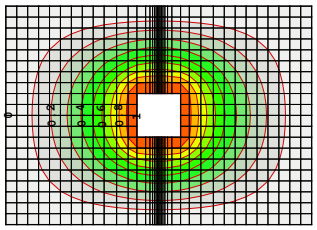

Figure 2: weighting coefficient calculated with a resolution of a lagrangian

4.1. Discretisations

In order to solve the structural problem, several behaviour laws have been studied. At first, a simple one, based on the isotropic case, has been implemented: $\vec{\vec{\sigma}} = 2\mu \vec{\vec{\epsilon}} + \lambda tr(\vec{\vec{\epsilon}})\mathbb{I}$
So we have :

$$\int\int\int_V div(\vec{\vec{\sigma}})dV = 0 \Longleftrightarrow$$

$$\int\int_S \mu \, grad\vec{\vec{U}} \,.\vec{n}\,dS + (\mu+\lambda)\, div(\vec{\vec{U}})\,.\vec{n}\,dS = 0$$

where $\vec{U}$ is the field of cell centers displacements, with

$$\begin{cases} \mu = \dfrac{E}{2(1+\nu)} \\ \lambda = \dfrac{\nu E}{(1+\nu)(1-2\nu)} \end{cases}$$

This first deformation approach is easy to implement, but does not allow to control the shear stress coefficient G (in this isotropic case $G = G_{iso}$). With this coefficient and the introduced structural anisotropy, one can theoretically maintain a rigid movement near the body and keep the orthogonality of cells near the body wall, a highly desirable property for finite-volume discretizations. Therefore, a 2D/3D volume finite discretisation using G has been developed :

For an orthotropical (orthogonal + anisotropic) material, the following behaviour law is given (hat notation) :

$$\hat{\sigma} = \begin{bmatrix} \sigma_x \\ \sigma_y \\ \sigma_z \\ \sigma_{xy} \\ \sigma_{yz} \\ \sigma_{xz} \end{bmatrix} = K \begin{bmatrix} 1 & \frac{\nu}{1-\nu} & \frac{\nu}{1-\nu} & 0 & 0 & 0 \\ \frac{\nu}{1-\nu} & 1 & \frac{\nu}{1-\nu} & 0 & 0 & 0 \\ \frac{\nu}{1-\nu} & \frac{\nu}{1-\nu} & 1 & 0 & 0 & 0 \\ 0 & 0 & 0 & \frac{G_{xy}}{K} & 0 & 0 \\ 0 & 0 & 0 & 0 & \frac{G_{yz}}{K} & 0 \\ 0 & 0 & 0 & 0 & 0 & \frac{G_{xz}}{K} \end{bmatrix} \begin{bmatrix} \epsilon_x \\ \epsilon_y \\ \epsilon_z \\ \epsilon_{xy} \\ \epsilon_{yz} \\ \epsilon_{xz} \end{bmatrix}$$

with $K = \frac{E(1-\nu)}{(1+\nu)(1-2\nu)}$ and $\epsilon_{xy} = \frac{1}{2}(\frac{\partial U}{\partial y} + \frac{\partial V}{\partial x})$ where G_{ij} is the shear stress coefficient in the $\vec{i}$ and $\vec{j}$ directions.

This symmetrical matrix gives an anisotropic discretisation with main directions. But the goal is to maintain the orthogonality of the mesh

around the structure during the deformation. So, one defines this matrix in a local basis $(\overrightarrow{n},\overrightarrow{t_2},\overrightarrow{t_3})$, with the vector $\overrightarrow{n}$ directed along the gradient vector of the weighting coefficient (their isovalues follow the body surfaces curves as shows in fig. 2). So the main deformation directions are local. And consequently one has a local behaviour depending to the local orientation of body surface. The general problem is expressed with the cartesian basis, so the behaviour law matrix must be rewritten in the cartesian basis.

Let P be the basis transformation matrix $(\overrightarrow{x},\overrightarrow{y},\overrightarrow{z})$ to $(\overrightarrow{n},\overrightarrow{t_2},\overrightarrow{t_3})$, one has :

$$\sigma_{(\overrightarrow{x},\overrightarrow{y},\overrightarrow{z})} = P\sigma_{(\overrightarrow{n},\overrightarrow{t_2},\overrightarrow{t_3})}P^{-1}$$

with

$$\overrightarrow{n} = n_x\overrightarrow{x} + n_y\overrightarrow{y} + n_z\overrightarrow{z}$$

$$P = \begin{bmatrix} n_x & P_{12} & P_{13} \\ n_y & P_{22} & P_{23} \\ n_z & P_{32} & P_{33} \end{bmatrix}$$

and consequently :

$$\widehat{\sigma} = \begin{bmatrix} \sigma_x \\ \sigma_y \\ \sigma_z \\ \sigma_{xy} \\ \sigma_{yz} \\ \sigma_{xz} \end{bmatrix} = K \begin{bmatrix} C_{11} & C_{12} & C_{13} & C_{14} & C_{15} & C_{16} \\ C_{12} & C_{22} & C_{23} & C_{24} & C_{25} & C_{26} \\ C_{13} & C_{23} & C_{33} & C_{34} & C_{35} & C_{36} \\ C_{14} & C_{24} & C_{34} & C_{44} & C_{45} & C_{46} \\ C_{15} & C_{25} & C_{35} & C_{45} & C_{55} & C_{56} \\ C_{16} & C_{26} & C_{36} & C_{46} & C_{56} & C_{66} \end{bmatrix} \begin{bmatrix} \epsilon_x \\ \epsilon_y \\ \epsilon_z \\ \epsilon_{xy} \\ \epsilon_{yz} \\ \epsilon_{xz} \end{bmatrix}$$

The C_{ij} coefficients have been calculated with MAPLE.

One notices that the G_{ij} coefficients are independent. G_{nt_2} and G_{nt_3} are chosen equal and stronger than the isotropic value, instead of $G_{t_2t_3}$ which is taken equal to $G_{iso} = \frac{E}{(1+\nu)}$. Therefore, the behaviour of a transverse isotropic material is obtained.

In order to have the mode implicit resolution of the problem, one rewrites the previous matrix so that the isotropic term appears :

$$\widehat{\sigma} = K \begin{bmatrix} 1 & \frac{\nu}{1-\nu} & \frac{\nu}{1-\nu} & 0 & 0 & 0 \\ \frac{\nu}{1-\nu} & 1 & \frac{\nu}{1-\nu} & 0 & 0 & 0 \\ \frac{\nu}{1-\nu} & \frac{\nu}{1-\nu} & 1 & 0 & 0 & 0 \\ 0 & 0 & 0 & \frac{G_{iso}}{K} & 0 & 0 \\ 0 & 0 & 0 & 0 & \frac{G_{iso}}{K} & 0 \\ 0 & 0 & 0 & 0 & 0 & \frac{G_{iso}}{K} \end{bmatrix} \widehat{\epsilon} + K\left[C - C_{iso}\right] \begin{bmatrix} \epsilon_x \\ \epsilon_y \\ \epsilon_z \\ \epsilon_{xy} \\ \epsilon_{yz} \\ \epsilon_{xz} \end{bmatrix}$$

The first matrix is calculated as the isotropic case (implicit calculation). The second matrix is explicitly taken into account.

This remeshing technique allows to update a grid around deformable (cf fig. 3) or undeformable bodies. With the use of the shear stress coefficient G one can maintain a rigid movement near the body and so keep the orthogonality of cells near the body wall. One has also the possibility to couple this regridding process with one of the others in order to obtain a better control of the deformation. This module uses the same discretisation tools as the fluid solver and the connectivities are identical. Moreover, the mesh deformation is entirely parallelized using MPI communication tools.

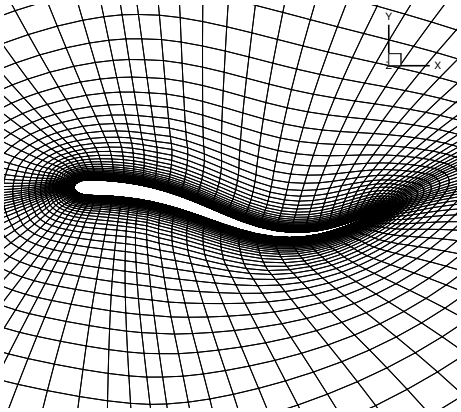

Figure 3: 3D meshes deformations around an eel-like body (ROBEA project) (cf A. Leroyer (2004))

5. THE STRUCTURAL SOLVER

5.1. Modelisation and hypothesis

With the distribution on the beam of the efforts exerted by the fluid, one can calculate its deformation, i.e. the displacements of its nodes. The structural solver is a "black box" based on the work of F. Boyer and D. Primault (cf F. Boyer (2004) and F. Boyer (2005)). The structural solver implemented into ISIS-CFD is based on the Cosserat approximation. The beam is considered as a monodimensional medium, built with a continuous stack of rigid micro-solid structures (cf E. and F. Cosserat (1909)). In this approximation, the beam sections must be rigid and plane. Without any other hypothesis, this kinematic is called "Timoshenko Reissner" (cf W. Weaver, Timoshenko and al (1990) and E. Reissner (1973)).

In our case, the beams are fine and elongated (cables, risers...). Then the Kirchoff hypothesis can be used with confidence : the beam sections are orthogonal to the neutral line of the beam. With this kinematic called "Kirchoff", two beam models are built : the "Rayleigh" model (cf L. Meirovitch (1967)) and the "Euler-

Bernoulli" model (cf L. Meirovitch (1967)). In this last model, the angular kinetic energy of the beam sections is neglected. With this simplification, the analytic equations are lighter. But a problem arises when the beam is free to rotate on itself.

The structural solver integrates both beam models resulting from the Kirchoff hypothesis : the "Rayleigh" and "Euler-Bernoulli" models.

5.2. The Euler-Bernoulli & Rayleigh kinematics

The Rayleigh kinematics (cf F. Boyer (2004) and F. Boyer (2005)) allow to solve correctly the cables problems thanks to the flexion-torsion coupling. Indeed the numerical solution is based on a variational formulation of the Kirchoff kinematics and on an exact modelisation of the most complex geometrical non-linearity : the flexion-torsion coupling (cf J.C. Alexander and Antman (1982)). An important notion appears here : the geometrically exact approach. This expression comes from Simo (cf J.C. Simo (1985)) and means that the approximations are done at the end of all the developments.

This kinematic needs a parametrisation. The rotation parametrisation is the most complex. In the Reissner kinematic case, the SO_3 Lie group is used. But the Kirchoff constraint reduces this space to a bidimensional SO_3 subspace. This one is parametrized by the position field of the beam neutral line and becomes the SO_2 plane rotations group. At first the rotation field is changed to the composition of two rotations : the movement of the beam neutral line only and the movement around this neutral line. Several parametrisations can be done for the rotation angles. In the implemented structural solver, the Eulerian parametrisation is used, due to its relative simplicity.

5.3. Validation test cases

5.3.1. Static validation

At first, in order to validate the solver implementation statically, a very simple 2D test case has been chosen: a beam with a uniform load. The implemented structural solver can treat the Euler-Bernoulli and Rayleigh kinetics which are compared with the help of this test case.

The comparison between the numerical and theoretical results shows that the solver consistently gives a numerical result which tends towards the theoretical value when the structural mesh is refined (cf tab. 1 and 2). With the Euler-Bernoulli kinetics, the convergence is 1.45 order for a load of 10 and 1.18 order for a load of 100. With the Rayleigh kinetics, the convergence is 1.2 order for a load of 10 and 1.6 order for a load of 100.

Load (q) Time step (h)	q=10	q=100
h=0.1	0.004907	0.048334
h=0.02	0.004252	0.043551
h=0.01	0.004312	0.042896
Theoretical value	0.0042857	0.042857

Table 1: *Euler-Bernoulli static validation (SI units).*

Load (q) Time step (h)	q=10	q=100
h=0.1	0.004837	0.048335
h=0.02	0.004369	0.043553
h=0.01	0.004320	0.042970
Theoretical value	0.0042857	0.042857

Table 2: *Rayleigh static validation (SI units).*

5.3.2. Dynamic validation

Then a dynamic validation has been performed : an embedded beam is loaded during a short period at the beginning, then is released in a fluid at rest (cf fig. 4). In the vacuum the beam will oscillate without damping at a frequency equal to the first theoretical eigenfrequency (cf C. Pertersen (1996)) :

$$f_1 = 0.5595 \frac{1}{L^2} \sqrt{\frac{EI}{m/L}}$$

In the following test-case the beam length L is set to $1m$, its thickness d to $0.01m$, its volumic

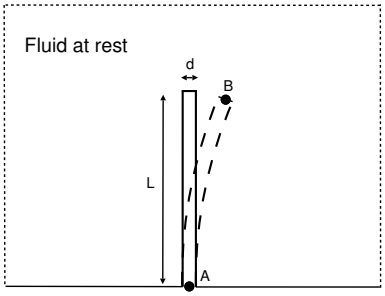

Figure 4: Free embedded (point A) beam in a fluid at rest

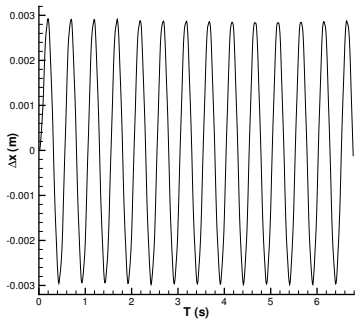

Figure 5: Oscillations of the point B in the vacuum

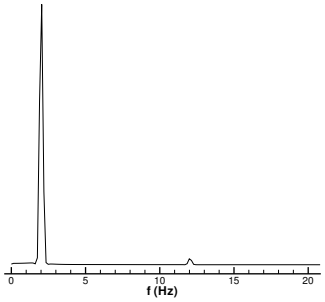

Figure 6: Eigenfrequencies of the beam oscillations

mass $\rho_{beam} = 2250\ SI$ and its Young modulus $E = 3500MPa$. Consequently, the theoretical first eigenfrequency f_1 is : $f_1 = 2.01Hz$. In the figure 5 we can see the evolution of the point B. The oscillations frequency is around $2.04Hz$ (cf fig. 6) which gives an relative error inferior to 2%.

When the beam oscillates in a fluid, like air or water, the oscillations are damped and this first eigenfrequency is modified. In air (with a viscosity set to $0.2\ SI$) this one is around $1.8Hz$. The higher is the fluid viscosity, the higher is the damping of the oscillations important.

5.4. First test-case and results

In this test-case the same embedded beam is used. But it is suddenly loaded by a constant incoming flow and oscillates as long as it reaches a steady deformation state (cf fig. 7). The test-case conditions are presented in the table 3. The resulting Reynold number is $Re = 50$.

The used fluid mesh is a totally unstructured mesh which contains around 30000 cells (cf fig. 8). The line which is the solid mesh is composed of 100 segments.

The time increment is $\delta t = 0.001s$ in order to

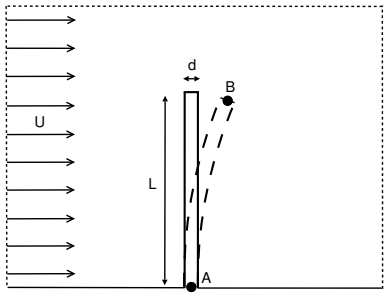

Figure 7: Embedded beam in a fluid in movement

Length	$L = 1\ m$
Thickness	$d = 0.01\ m$
Young modulus	$E = 3500\ MPa$
Solid volumic mass	$\rho_s = 1200\ kg\ m^{-3}$
Fluid volumic mass	$\rho_f = 1\ kg\ m^{-3}$
Dynamic viscosity	$\mu_f = 0.2\ Pa\ s$
Constant inflow velocity	$U = 10\ m\ s^{-1}$

Table 3: *Test-case conditions (SI units).*

reach approximatively more than 300 time steps per oscillation period, which is a good value to have a good accuracy.

The results show that the beam oscillates during several seconds and then finds a steady state. The free extremity (point B) moves aproximatively $1.5cm$ from the free steady state (cf fig. 9). The flow at the steady state has a big recirculation to the rear of the beam and two little on each sides (cf fig. 10).

6. CONCLUSION

In this paper the methods to perform simulations coupling a RANSE solver with a structural solver for elongated bodies in large deformations and

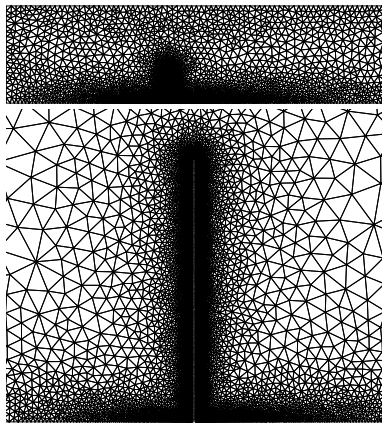

Figure 8: Mesh around the beam and far away

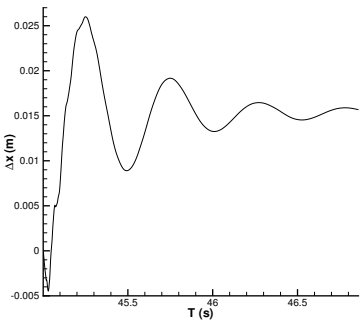

Figure 9: Oscillations of the point B in the fluid

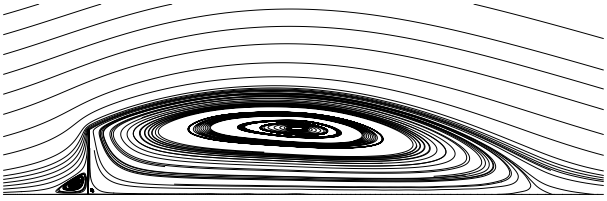

Figure 10: Flow around the deformed beam at the steady state

large displacements have been presented. This one is based on the Cosserat hypothesis with the Rayleigh or Euler-Bernoulli kinematics.

A general remeshing procedure is also detailed. This one is based on the pseudo-solid approximation and allows to control the mesh deformation through a particular local behaviour law.

First the 3D structural solver was verified with 2D standard test-cases. Then the coupled code was used to an example with 2D simple geometry.

In the future in order to improve the FSI into ISIS-CFD, the replacement of the Newmark algorithm for the time integration is planned, because it gives some high frequencies perturbations. More validation 2D & 3D test-cases will be performed with comparisons to experimental data.

7. REFERENCES

P. Spalart and S. Allmaras, 1992, A one-equation turbulence model for aerodynamic flows. In *AIAA 30th Aerospace Sciences Meeting* **92**: 0439.

F.R. Menter, 1993, Zonal two-equation $k-\omega$ turbulence models for aerodynamic flows. In *AIAA 24th Fluid Dynamics Conference*: 93-2906.

G.B. Deng and al, 2005, Three-dimensional flow computation with Reynolds stress and algebraic stress models. In *Proceedings of the ERCOFTAC International Symposium on Engineering Turbulence Modelling and Measurements* : 389-398.

A. de Boer et al., 2007, Review of coupling methods for non-matching meshes. In *Comput. Methods Appl. Mech. Engrg.* **196**: 515-1525.

A. Leroyer and M. Visonneau, 2005, Numerical methods for RANSE simulations of a self-propelled fish-like body. In *Journal of Fluids and Structures* **20**: 975-991.

A. Leroyer, 2004, Etude du couplage écoulement/mouvement pour des corps solides ou à déformation imposée par résolution des équations de Navier-Stokes. Contribution à la modélisation numérique de la cavitation. $ftp://ftpa.ec-nantes.fr/pub/DMN/Thesis/these\_leroyer.pdf$

F. Boyer and D. Primault, 2004, Finite element of slender beams in finite transformations : a geometrically exact approach. In *International Journal for numerical methods in engineering* **59**: 669-702.

F. Boyer and D. Primault, 2005, Finite element of non-linear cables : applications to robotics. In *Far East Journal of Applied Mathematics* **19**: 1-34.

E. and F. Cosserat, 1909, Théorie des corps déformables. Hermann, Paris.

W. Weaver, Timoshenko and al, 1990, Vibrations problems in engineering. John Wiley & Sons, New York.

E. Reissner, 1973, On a one-dimensional large displacement finite-strain theory. Stud. Appl. Math. **52**: 87-95.

L. Meirovitch, 1967, Analytical methods in vibrations. Mc Millan Publish., New York.

J.C. Alexander and Antman, 1982, The anbiguous twist of Love. In *Quaterly of Applied mathematics* **2**: 83-92.

J.C. Simo, 1985, A finite strain beam formulation. The three-dimensional dynamic problem. Part I. In *Comp. Meth. Appl. Mech. Eng.* **49**: 55-70.

C. Pertersen, 1996, Dynamik der Baukonstruktionen. Vieweg, Braunschweig/Wiesbaden.